# SUPPLEMENTARY INFORMATION

## 1. Raindrop Uptake of Noble Gas Model

We assume an initial uniform concentration defined as $C_1$ and a drop radius of $a$, which is half of the drop diameter. As the drop falls, its velocity will decrease as the ambient pressure rises. The simplified model of Best (1950) was used for raindrop terminal velocity instead of more precise models proposed later (e.g. Foote and Du Toit, 1969) as it has the advantage that the formulation does not produce a negative terminal velocity event for extremely small drop diameters.

The simplified atmosphere pressure model used in Ballentine and Hall (1999) was employed, where $P_0 = e^{-H/h_0}$, altitude is $H$and the scale height $h_0$ is 8350m. Also, an initial uniform concentration is defined as $C_1$.

The model assumes a linear rise in temperature as the drop falls (i.e., a constant lapse rate), and we assume that the drop is always at the same temperature as the surrounding air. In addition, we assume that transport into and within a raindrop is due solely to diffusion, i.e., there is no mechanical mixing of concentrations within a raindrop. This is a gross simplification, but it does mean that our noble gas uptake model is extremely conservative in that it will always underestimate the dissolution of noble gases compared to the case of water stirring within the drop due to air friction. Thus, all of the estimates of noble gas concentrations derived from this model should be regarded as minimum estimates of noble gas exchange.

Diffusive uptake of noble gases is based on eqn 3 in section 9.3 of Carslaw and Jaeger, translated into diffusion instead of heat conduction:

$$\begin{aligned} C(r,t) &= \frac{2}{ar}\sum_{n=1}^{\infty} e^{-Dn^2\pi^2 t/a^2}\sin\frac{n\pi r}{a} \\ &\quad \times\left\{\int_0^a r' f(r')\sin\frac{n\pi r}{a}dr' - n\pi D(-1)^n\int_0^t e^{Dn^2\pi^2\lambda/a^2}\phi(\lambda)d\lambda\right\} \end{aligned} \tag{1}$$

The first term on the second line is the solution for the case with zero boundary condition but initial concentration profile given by $f(r)$. The second term on the second line is a solution with zero initial concentration, but with the boundary condition that the surface concentration as a function of time is given by $\phi(t)$. The sum of the two terms is guaranteed to have the appropriate initial condition and the correct boundary condition for all times.

In our case, $D$ is a function of time as well, which complicates matters, but fortunately, Crank (1979) points out that it is still possible use the constant $D$ solutions if we replace time by $\tau$, with

$$\tau = \int_0^t D(t')dt' \tag{2}$$

So the above general equation is just the same, but using $\tau$ instead of $t$ and setting $D$ to 1.

In general, it is not practical to attempt an analytical solution for the above equation because not only is temperature a complex function of time and $\tau$, but the boundary condition (ASW) is in turn a complex non-linear function of temperature. We can, however, approximate $\phi(\tau)$ by subdividing the atmosphere into $j$ thin layers and approximate the function as being made up of linear segments at locations 0 through $j$. Currently, the software divides the atmosphere between the beginning altitude and the collection altitude into $j = 10000$ layers. At each level $i$, a diffusion coefficient $D_i$ is defined by the lapse rate determined temperature $T_i$. The atmospheric pressure $P_i$ defines the local drop velocity $v_i$ and this helps to define the timeline of the drop's fall. The time $t_i$ is given by:

$$t_i = \sum_{k=1}^{i} \frac{d_l}{(0.5 \times (v_k + v_{k-1}))} \tag{3}$$

Here $d_l$ is the atmospheric layer thickness. The integral of the diffusion coefficient with time is approximated by:

$$\tau_i = \sum_{k=1}^{i} (t_k - t_{k-1}) \frac{(D_k + D_{k-1})}{2} \tag{4}$$

The boundary condition as a function of the layer number can be calculated as:

$$\phi_i = ASW(T_i, P_i) \tag{5}$$

The boundary condition function is approximated by linear segments at each of the layer boundary points. The critical issue is the second major term in the first equation that deals with the integral of the boundary condition as a function of time. Let us define a new function $\Lambda(\tau)$ to be

$$\Lambda(\tau) = \int_0^{\tau} e^{n^2\pi^2\lambda} \phi(\lambda) d\lambda \tag{6}$$

In the interval from $\tau_{i-1}$to $\tau_i$, the boundary condition is approximated as:

$$\phi(\lambda) = m_i\lambda - m_i\tau_{i-1} + \phi_{i-1} \tag{7}$$

Here $m_i = \frac{\phi_i - \phi_{i-1}}{\tau_i - \tau_{i-1}}$and it is the slope of the boundary condition function from $\tau_{i-1}$to $\tau_i$. The integral can then be approximated by:

$$\Lambda(\tau_j) = \sum_{i=1}^{j} \int_{\tau_{i-1}}^{\tau_i} e^{n^2\pi^2\lambda} \phi(\lambda) d\lambda = \sum_{i=1}^{j} d\Lambda_i \tag{8}$$

The linear segment integral is:

$$d\Lambda_i = \frac{a^2}{n^2\pi^2} e^{n^2\pi^2\tau_i/a^2} \left\{ \phi_i - m_i \frac{a^2}{n^2\pi^2} \right\} - \frac{a^2}{n^2\pi^2} e^{n^2\pi^2\tau_{i-1}/a^2} \left\{ \phi_{i-1} - m_i \frac{a^2}{n^2\pi^2} \right\} \tag{9}$$

A numerical approximation to the first equation can be written as:

$$C(r,\tau_j) = \frac{2}{ar}\sum_{n=1}^{\infty} e^{-Dn^2\pi^2\tau_j/a^2}\sin\frac{n\pi r}{a}\times \times\left\{\frac{-C_1a^2}{n\pi}(-1)^n - n\pi(-1)^n\sum_{i=1}^{j} d\Lambda_i\right\} \quad (10)$$

The average concentration at interval $\tau_j$ is given by:

$$\begin{aligned} C_{av}(\tau_j) &= \frac{3}{4\pi a^3}\int_0^a 4\pi r^2 C(r,\tau_j)dr \quad (11)\\ &= \frac{6}{\pi^2}C_1\sum_{n=1}^{\infty}\frac{1}{n^2}e^{-n^2\pi^2\tau_j/a^2} \\ &\quad +\frac{6}{\pi^2}\sum_{i=1}^{j}\sum_{n=1}^{\infty}\frac{1}{n^2} \\ &\quad \times\left\{e^{n^2\pi^2(\tau_i-\tau_j)/a^2}\left(\phi_i - m_i\frac{a^2}{n^2\pi^2}\right) - e^{n^2\pi^2(\tau_{i-1}-\tau_j)/a^2}\left(\phi_{i-1} - m_i\frac{a^2}{n^2\pi^2}\right)\right\} \end{aligned}$$

The first part of the equation deals with the initial conditions and the second part deals with the variable boundary conditions.

In addition to the figure shown in the main text, figures S1 through S4 below are the results of simulated uptake of noble gases at different lapse rates and at different temperatures at a collection altitude of 1000m.

## 2. ES Cluster Buoyancy Near the Surface of a Droplet

The internal pressure increase within a droplet of radius $a$ is given by:

$$\Delta P_{YL} = \frac{2\gamma}{a} \quad (12)$$

Here $\gamma$ is the surface tension of water. At 15°C, $\gamma$ is about 73.5 mN/m, and therefore a droplet with a diameter of 3$\mu$m will have a pressure increase within the interior near 1 atmosphere (98000 Pa, or 0.98 Bar) above ambient atmospheric pressure. If one assumes that liquid water is composed of a mixture of expanded structure (ES) clusters and condensed structure (CS) clusters, then ES clusters, being lower density than the aggregate mixture of ES and CS clusters should feel a buoyancy force in a manner completely analogous to that of material floating in liquid water (e.g., Archimedes principle). If the bulk water density is given as $\rho_w$ and the ES cluster density is $\rho_E$, then the force pushing an ES cluster of mass $m_E$ toward the surface of the droplet should be:

$$F_E = m_E\frac{dP}{dr}\left(\frac{1}{\rho_E} - \frac{1}{\rho_w}\right) \quad (13)$$

In this equation, $\rho_w$ is the local water density. It will be the bulk density of water at the interface between the interior of the droplet, where the pressure is highest. Further out, if the mass fraction of ES clusters increases due to the buoyancy effect, the local value of $\rho_w$ will diminish, thereby reducing the outward force on the ES cluster.

If one assumes that the Young-Laplace pressure is distributed over roughly 2 nm, then for a 3 $\mu$m diameter droplet, the pressure gradient would be $4.9 \times 10^{13}$Pa/m, which is equivalent to the acceleration induced pressure gradient in water from a centrifuge with a centripetal acceleration of 5 billion $g$!

Conversely, CS clusters within the boundary layer with a significant pressure gradient will feel a force causing them to sink inward toward the interior of the droplet. The force at the boundary between the outer layer and the droplet interior is given by:

$$F_C = m_c \frac{dP}{dr}\left(\frac{1}{\rho_w} - \frac{1}{\rho_C}\right) \tag{14}$$

As before, as ES clusters migrate outward to the surface of the droplet, the local $\rho_w$ will diminish until the mass fraction of CS clusters approaches zero. At this point, the maximum inward force on a CS cluster would be:

$$F_{Cmax} = m_C \frac{dP}{dr}\left(\frac{1}{\rho_E} - \frac{1}{\rho_C}\right) \tag{15}$$

One can estimate the average drift velocity for an ES or CS cluster by employing equations 13 to 15 along with Stoke's Law. Following Roos (2014):

$$F_{drag} = 6\pi\mu R v \tag{16}$$

where $\mu$ is the kinematic viscosity of water, $R$ is the radius of the cluster and $v$ is the velocity. Equating $F_{drag}$ to the buoyancy forces above, one can solve for the velocity $v$.

The pressure gradient within the interior of the droplet should drop dramatically near the surface at $r = a$ and one can imagine that there is a radial position $r_i$ within which the pressure gradient can be assumed to be zero. The potential energy lost for an ES cluster mass $m_E$ moving from $r_i$ to the droplet surface will be

$$\begin{aligned}
\Delta U_E &= -\int_{r_i}^{a} m_E \frac{dP}{dr}\left(\frac{1}{\rho_E} - \frac{1}{\rho_w}\right) \\
&= m_E \left(\frac{1}{\rho_E} - \frac{1}{\rho_w}\right) P_{YL} \\
&= \frac{2\gamma m_E}{a}\left(\frac{1}{\rho_E} - \frac{1}{\rho_w}\right)
\end{aligned} \tag{17}$$

and the potential energy lost when a CS cluster sinks from the surface into the interior is

$$\begin{aligned}
\Delta U_C &= -\int_{r_i}^{a} m_C \frac{dP}{dr}\left(\frac{1}{\rho_w} - \frac{1}{\rho_C}\right) \\
&= m_C \left(\frac{1}{\rho_w} - \frac{1}{\rho_C}\right) P_{YL} \\
&= \frac{2\gamma m_C}{a}\left(\frac{1}{\rho_w} - \frac{1}{\rho_C}\right)
\end{aligned} \tag{18}$$

If a CS cluster forms at a droplet surface that is populated entirely by ES clusters, then its potential energy relative to being in the interior of the droplet is given by

$$\Delta U_{Cmax} = \frac{2\gamma m_C}{a}\left(\frac{1}{\rho_E} - \frac{1}{\rho_C}\right) \tag{19}$$

This potential energy would also be released if the CS cluster transformed its structure into that of an ES cluster. Thus, it may not be necessary for clusters to be transported within the droplet for the Young-Laplace pressure gradient to promote the formation of a surface layer that is rich in ES clusters.

By making some simplifying assumptions, it is possible to make a rough estimate of the thickness of an ES-rich shell that could form on the surface of a water droplet. As with Vedamuthu et al. (1994), we assume that water clusters are either an ES variety with minimal density or the CS variety with maximal density, without a range of configurations in between. Second, we assume that the Laplace-Young pressure gradient is distributed uniformly across a thin shell of thickness $t$. Finally, given a constant temperature and pressure, no external work is done and thus the shell thickness will form with no change in the Gibbs free energy relative to a droplet with zero surface tension. The change in enthalpy will be the same as the change in potential energy, but averaging across the entire shell, the change in potential energy for the movement of clusters will be half that given in equations 17 and 18. Also, for small diameter droplets, the movement of CS clusters into the interior and ES clusters to the surface may slightly increase the water density in the interior of the droplet.

The thickness of the surface ES-rich layer is nearly independent of droplet size. This can be undersood because although the mass of material involved in forming the shell is proportional to $a^2t$, where $a$ is the droplet radius, the pressure gradient is proportional to $1/a$. Therefore the enthalpy change for the droplet is proportional to $at$. Assuming that the entropy change is proportional to the natural logarithm of the reduction of volume allowed for CS clusters, i.e., they now are confined within a sphere with radius $a - t$, then $\Delta$S will be proportional to $\ln\left((a-t)/a\right)^3)$, which simplifies to $3\ln\left(1 - t/a\right)$. To an excellent approximation, when $t \ll a$, this expression equals $-t/a$. Therefore, $\Delta$S times the mass of CS clusters confined within the interior of the droplet is propotional to $at^2$. To a first approximation, the thickness that satisfies $\Delta$G=0 can be given by:

$$at = \Upsilon at^2 \tag{20}$$

where the constant $\Upsilon$ is only weakly dependent on droplet diameter and temperature. Figure S5 shows $\Delta$G as a function of shell thickness for three different droplet diameters and they all cross the $\Delta$G=0 line at virtually the same thickness value. Although the ES-rich shell thickness should be virtually independent of droplet size, the energy released per mole of clusters in the shell is proportional to $at/a^2t$, or just $1/a$. Figure S6 displays the expected release in enthalpy per mole of water molecule clusters as a function of droplet diameter. Note that there is a dramatic reduction in the enthalpy release for droplets larger than about 10 μ. This suggests that only the smallest droplets will have well defined and coherent ES-rich shells that can resist the effects of random thermal fluctuations.

## 3. Xenon Isotopic Fractionation

Xenon has a large number of isotopes and it has displayed both mass depentent fractionation (MDF) as well as mass independent fractionation (MIF) in a variety of settings (e.g., Robert, 2004; Thiemens, 2006). Xenon isotopic fractionation was calculated for the subset of isotopes with masses 128, 129, 130, 131, 132, 134 and 136. Rather than plot deviations from an expected isotopic ratio based on a single reference isotope (e.g.$^{132}$Xe), the fractional isotopic composition of the entire set of measured Xe isotopes was calculated and then compared with the expected fraction of the isotope within the same set for a standard air sample. This avoids the problem that the reference isotope in the denominator of the ratios may itself be subject to MIF. Thus, all isotopes are treated equally and patterns for all of the measured isotopes can be revealed independently.

Figure 7 shows the results of all of the measured samples, except PR 3/24-15a, which was measured using the Thermo Helix SFT mass spectrometer. Its Xe isotopic ratio data are not nearly as precise as the data collected later from the Thermo Argus VI. Results are plotted as parts per thousand (‰) deviations from the atmospheric Xe composition. Average fractionation values for the isotopes are plotted as a green line along with estimated $\pm 1\sigma$ errors marked as dashed green lines. For both Puerto Rico and Shenandoah samples, masses 132, 134 and 136 are essentially unfractionated, while the two lighter isotopes that have an even number of nucleons are significantly depleted. The deviation at mass 130 explains the departure of the plotted Xe isotope ratios from the MDF line seen in Figure 4d of the main text. Note that the two odd numbered isotopes (129 and 131) are significantly enriched relative to the neighboring even numbered isotopes (128, 130, 132). This might be due to optical effects that can become important for atoms with a non-zero nuclear spin, as is the case for Hg isotopes (Bergquist and Blum, 2009). In any case, the complex fractionation pattern for Xe isotopic solubility in cloud water suggests that there are important interactions that take place on the surface of droplets and that this effect might be enhanced if small droplets have a relatively rigid skin of ES molecular clusters.

## 4. Disclaimer

Any use of trade, firm, or product names is for descriptive purposes only and does not imply endorsement by the U.S. Government.

## 5. References

Ballentine, C.J. and Hall, C.M., 1999. Determining paleotemperature and other variables by using an error-weighted, nonlinear inversion of noble gas concentrations in water. Geochimica et Cosmochimica Acta, 63(16), pp.2315-2336.

Bergquist, B.A. and Blum, J.D., 2009. The odds and evens of mercury isotopes: applications of mass-dependent and mass-independent isotope fractionation. Elements, 5(6), pp.353-357.

Best, A.C., 1950. Empirical formulae for the terminal velocity of water drops falling through the atmosphere. Quarterly Journal of the Royal Meteorological Society, 76(329), pp.302-311.

Carslaw, H.S. and Jaeger, J.C., 1959. Conduction of heat in solids. Oxford: Clarendon Press, 1959, 2nd ed.

Crank, J., 1979. The mathematics of diffusion. Oxford University Press.

Foote, G.B. and Du Toit, P.S., 1969. Terminal velocity of raindrops aloft. Journal of Applied Meteorology, 8(2), pp.249-253.

Roos, N., 2014. Entropic forces in Brownian motion. American Journal of Physics, 82(12), pp.1161-1166.

Robert, F., 2004. The common property of isotopic anomalies in meteorites. Astronomy & Astrophysics, 415(3), pp.1167-1176.

Thiemens, M.H., 2006. History and applications of mass-independent isotope effects. Annu. Rev. Earth Planet. Sci., 34, pp.217-262.

Vedamuthu, M., Singh, S. and Robinson, G.W., 1994. Properties of liquid water: origin of the density anomalies. The Journal of Physical Chemistry, 98(9), pp.2222-2230.

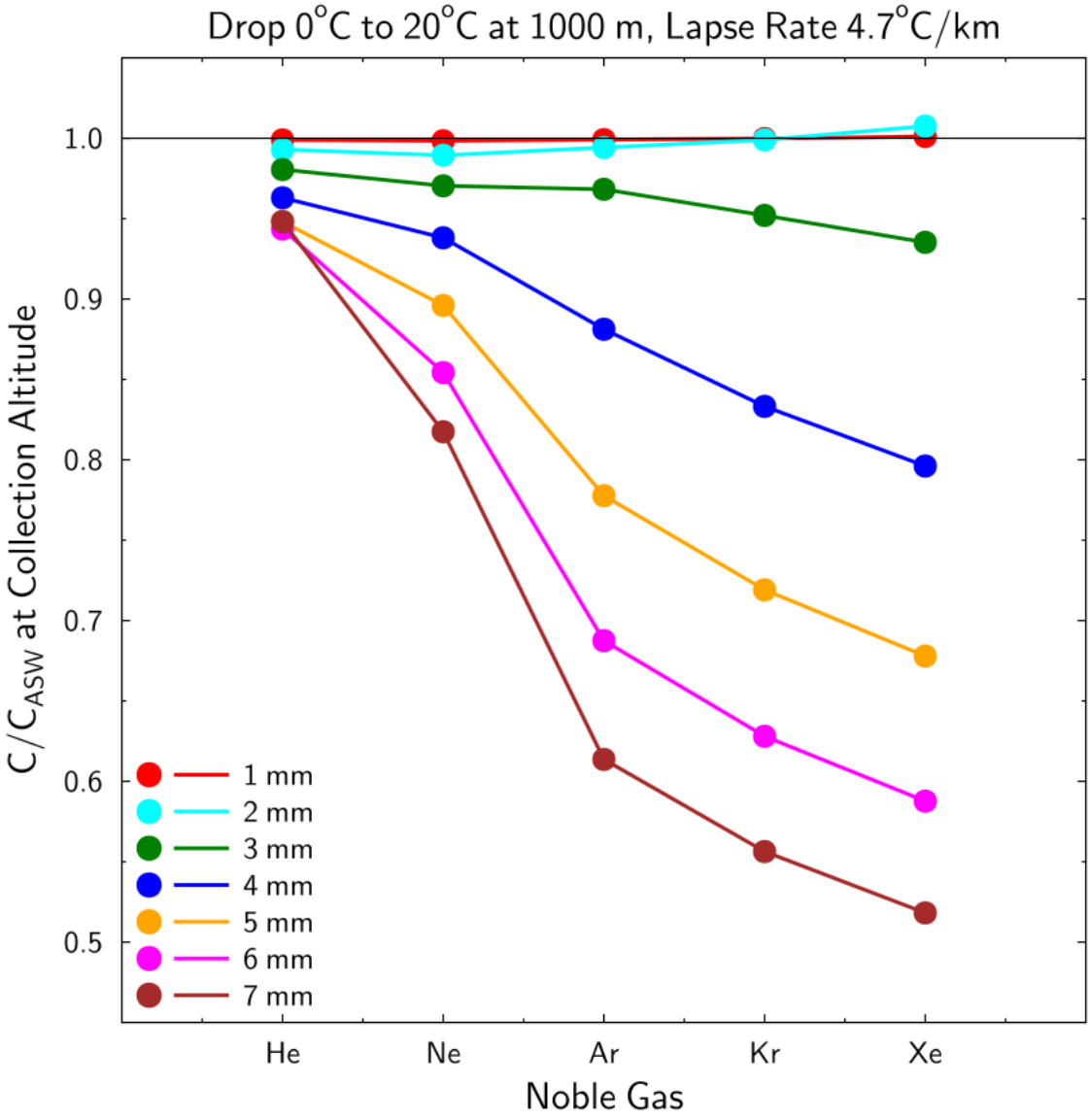


FIGURE S1. Simulated uptake of noble gases with a collection point altitude of 1000m and a temperature of $20^0$C assuming a wet lapse rate of $4.7^0$C per km.

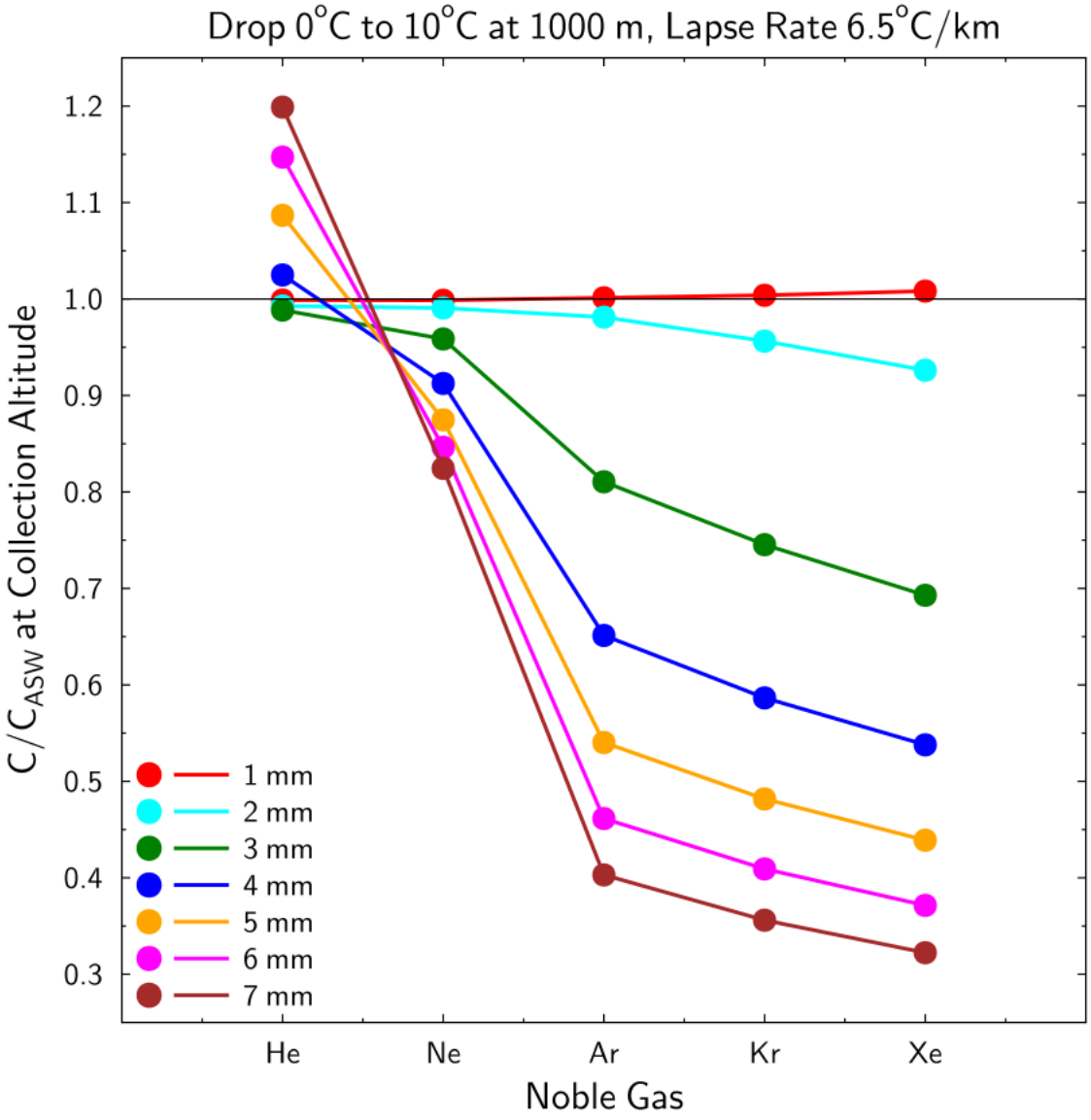


FIGURE S2. Modeled uptake of noble gases from snow that melts and falls to an altitude of 1000m at a collection point temperature of 10°C. Lapse rate is 6.5°C per km.

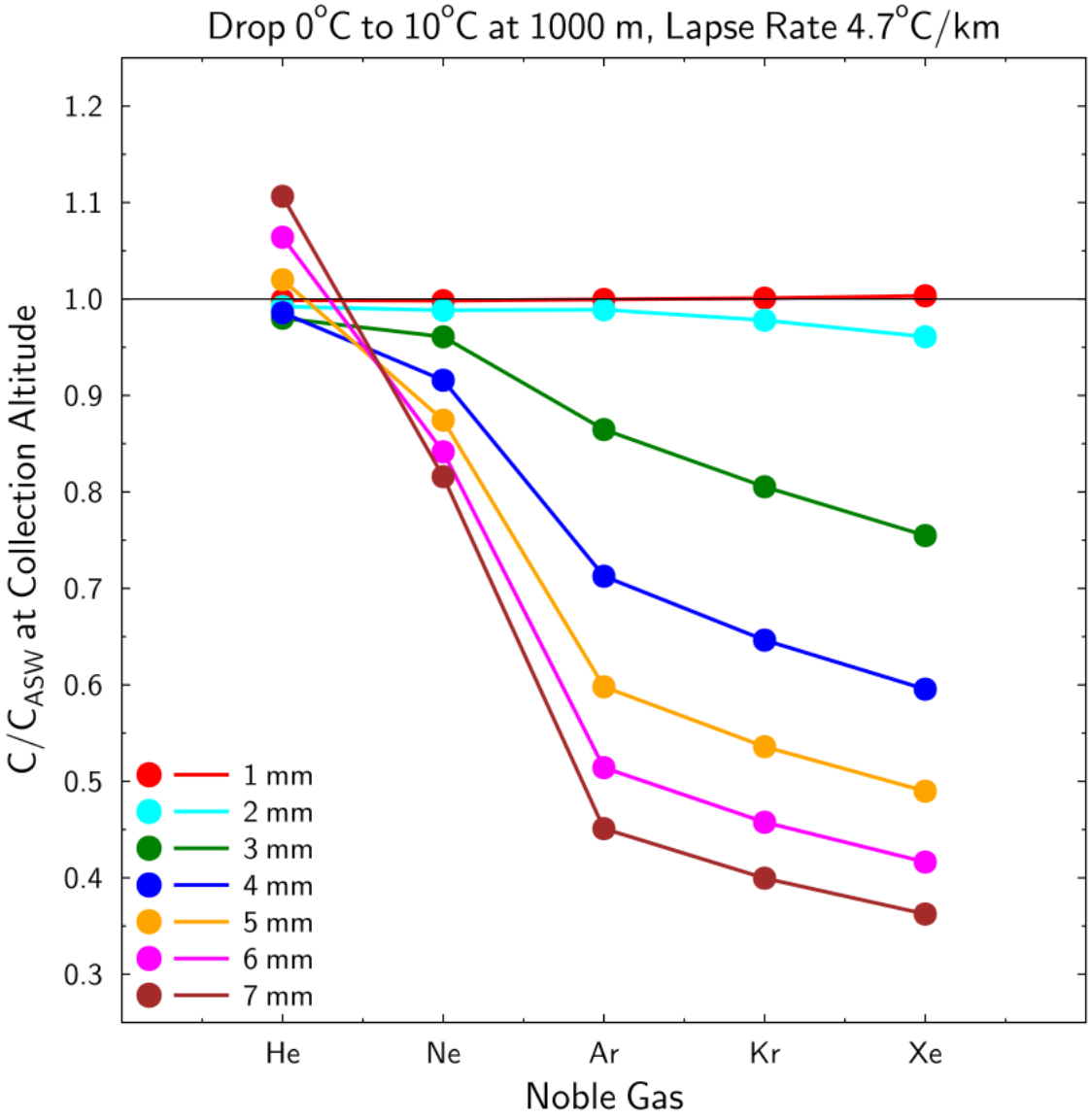


FIGURE S3. Modeled uptake of noble gases from snow that melts and falls to an altitude of 1000m at a collection point temperature of 10°C. Lapse rate is 4.7°C per km.

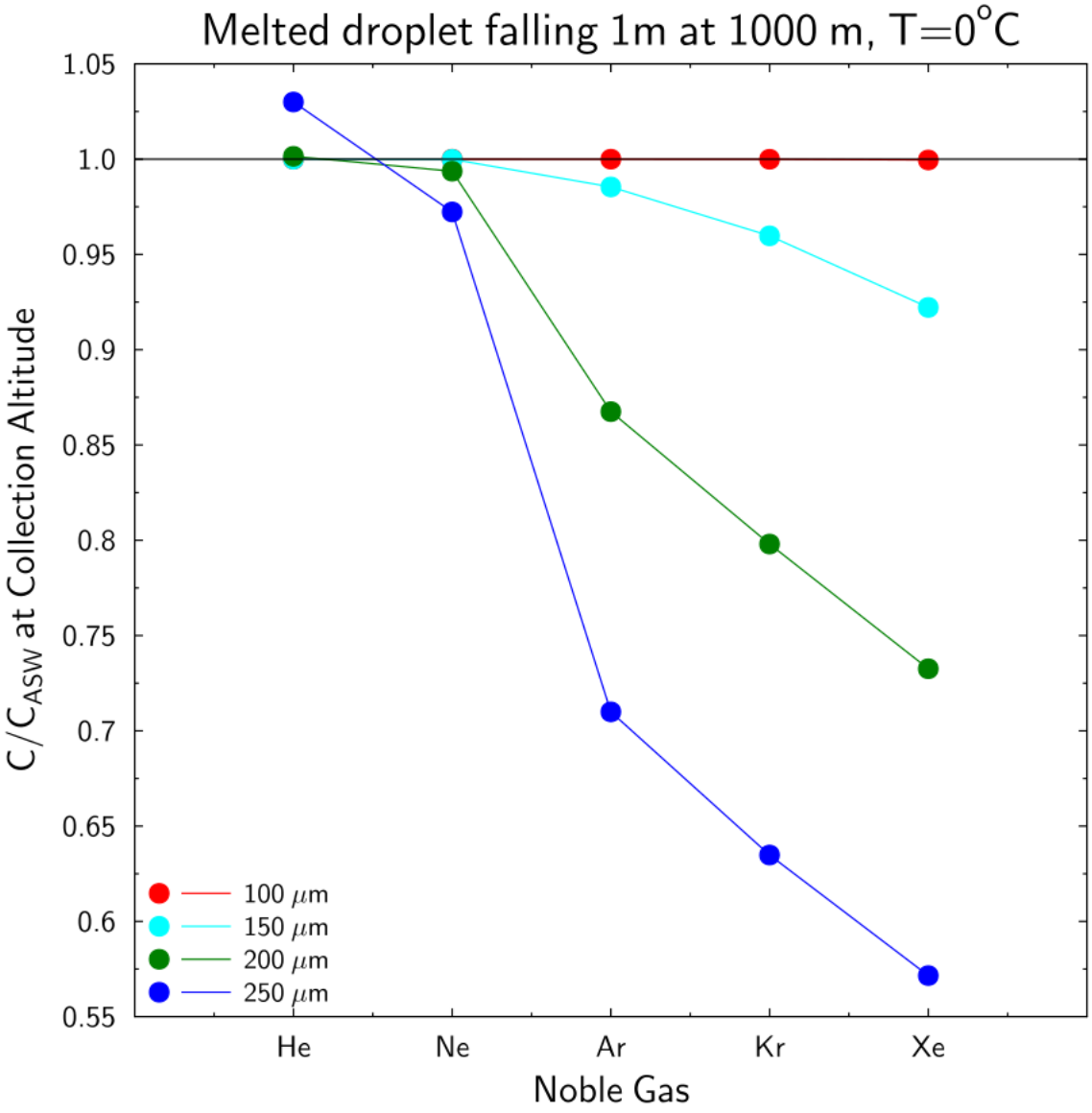


FIGURE S4. Modeled uptake of noble gases from snow that melts and falls only 1m to an altitude of 1000m at a collection point temperature of 0°C.

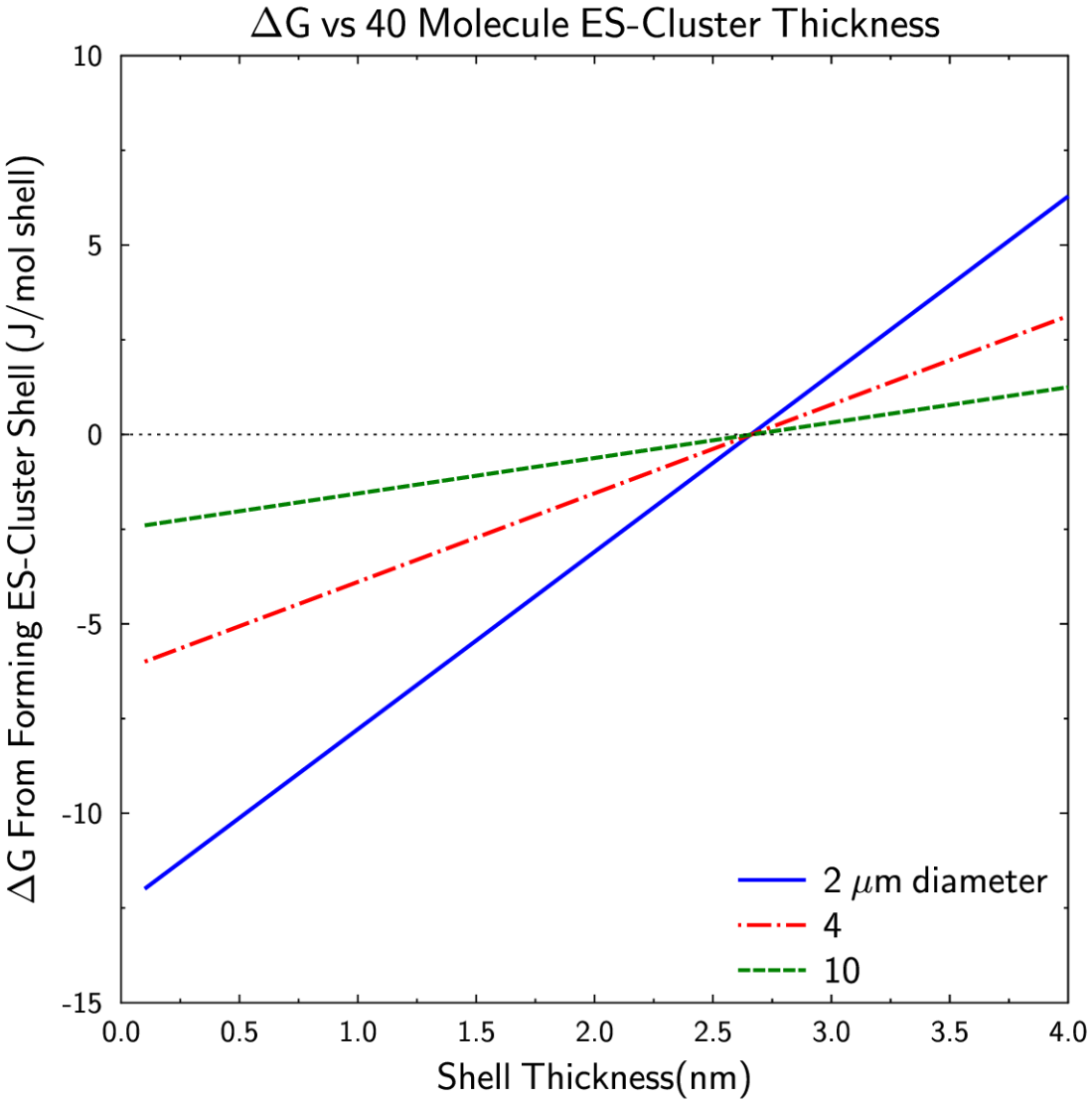


FIGURE S5. ΔG as a function of ES shell thickness for three different droplet diameters using the assumptions in the text. T=15°C and the assumed cluster size is 40 water molecules. The ES-rich shell should grow until ΔG=0, at a thickness of about 2.66 nm.

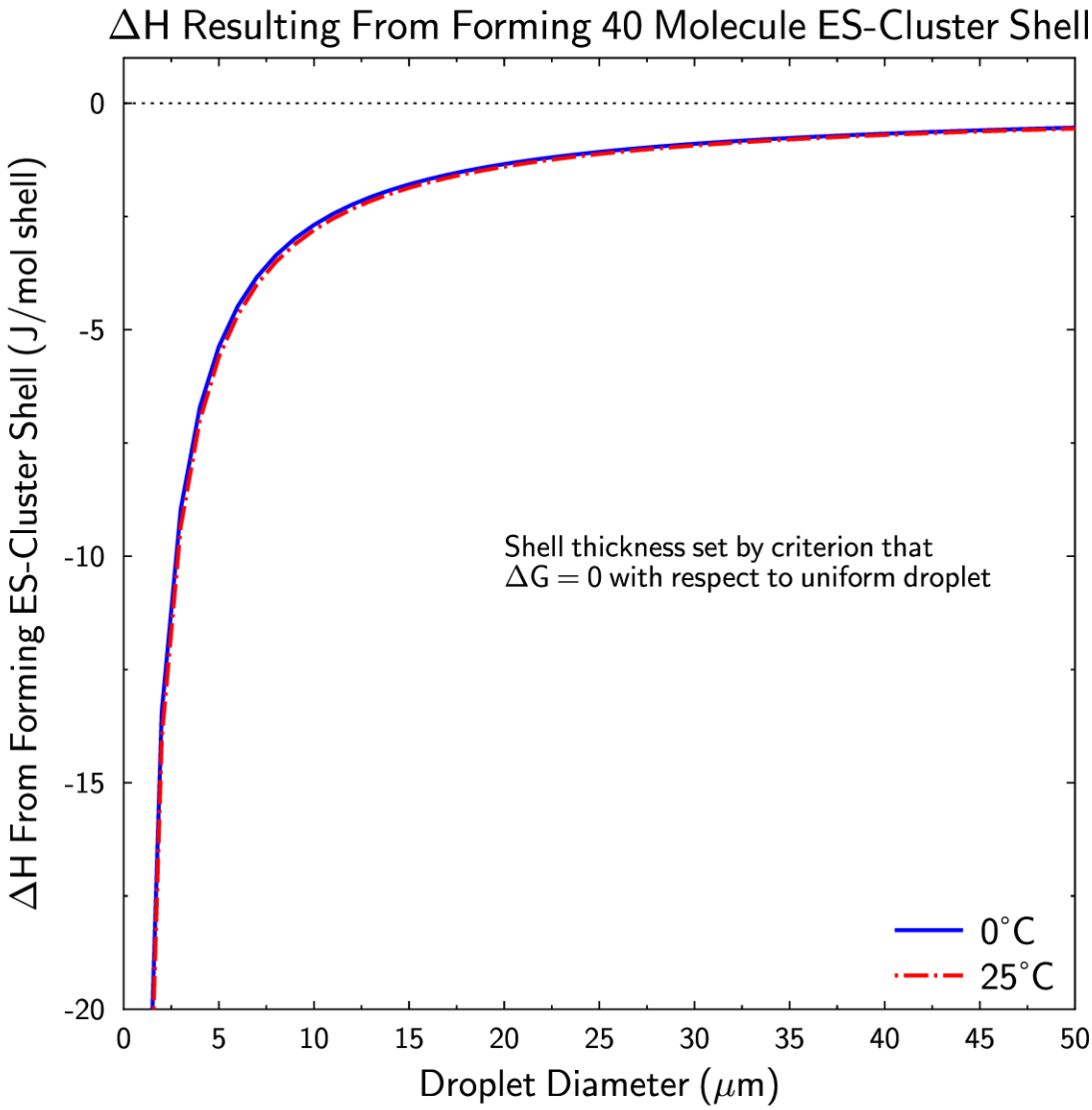


FIGURE S 6. ΔH per mole of water clusters from the formation of an ES cluster shell as a function of droplet diameter. Assumed water cluster size is 40 molecules. Values are given for two different temperatures.

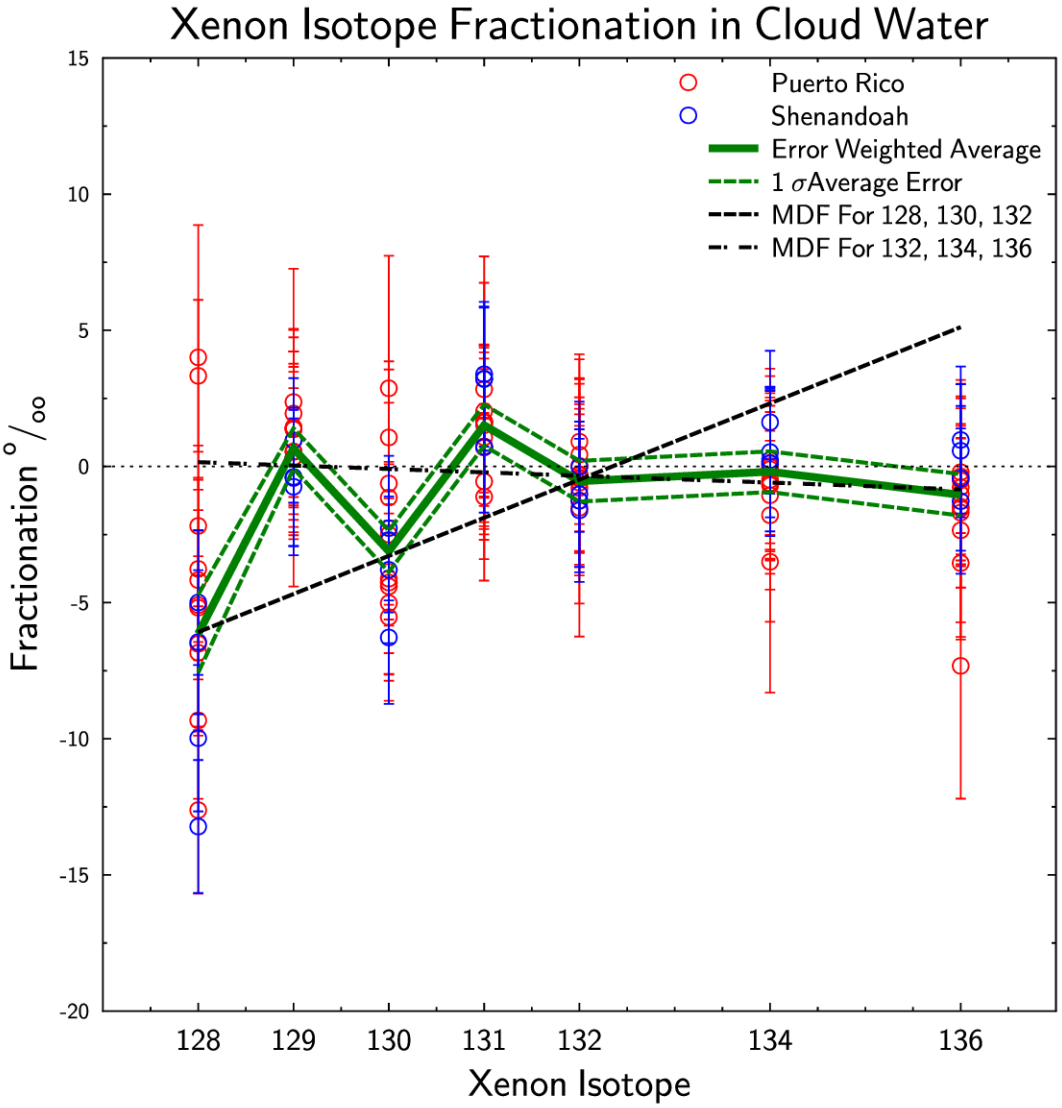


FIGURE S7. Fractionation pattern for the cloud water samples. See text for the method of calculation. Black dashed best fit lines are displayed for average MDF patterns for a selection of even numbered masses, one for 128, 130 and 132 along with one for 132, 134 and 136. The former set shows a possible MDF enriched in heavy isotopes and the latter shows virtually no fractionation between the 3 heaviest isotopes. The two odd numbered isotopes are distinctly enriched relative to their even numbered neighbors. All error estimates $1\sigma$.